

Spin Model for Quantum Annealing with Kerr Parametric Oscillators

Leo Stenzel,^{1,*} Roeland ter Hoeven,² Ryoji Miyazaki,^{3,4} Tomohiro Yamaji,^{3,4} Masayuki Shirane,^{3,4} and Wolfgang Lechner^{2,5}

¹*Parity Quantum Computing Germany GmbH, Schauenburgerstraße 6, 20095 Hamburg, Germany*

²*Parity Quantum Computing GmbH, Rennweg 1, Top 314, 6020 Innsbruck, Austria*

³*Secure System Platform Research Laboratories, NEC Corporation, Kawasaki, Kanagawa 211-0011, Japan*

⁴*NEC-AIST Quantum Technology Cooperative Research Laboratory, Tsukuba, Ibaraki 305-8568, Japan*

⁵*Institute for Theoretical Physics, University of Innsbruck, 6020 Innsbruck, Austria*

(Dated: March 13, 2026)

Coherent states offer a promising path for near-term quantum computing due to their inherent protection against bit-flip noise. However, their large photon numbers can be challenging for numerical simulation. This paper introduces an effective model, representing coherent-state quantum annealing using spin-1/2 degrees of freedom. We demonstrate that this model yields accurate predictions for realistic experimental settings and can therefore serve as a practical tool for optimizing future quantum hardware.

I. INTRODUCTION

Quantum computing technology has advanced rapidly and has been implemented in several ways. One promising platform is superconducting circuits. Their high degree of tunability enables us to generate energy structures in which the circuit states are confined to two specific states, making them suitable for use as qubits [1]. While a representative example of a superconducting qubit relies on the vacuum and single-photon states [2], coherent states readily generated in superconducting circuits are also known to function as distinctive qubits due to their robustness against single-photon loss and phase-flip errors [3–5]

One prominent application of quantum computations with coherent states is quantum annealing [6–8] using Kerr parametric oscillators (KPOs) in superconducting circuits [9–13]. In this approach, the KPOs system evolves under parametric driving to a superposition of coherent states, whose relative phases correspond to the solution of an embedded Ising problem. The efficiency of KPO-based quantum annealing has been numerically demonstrated for small systems [9, 10, 14]. This scheme can also be utilized for Boltzmann sampling [15] and quantum annealing using excited states [16, 17]. In addition, KPO-based quantum annealing is particularly well suited [10] for building the so-called Parity architecture [18–22], which enables problem-specific connectivity, including the all-to-all one, of logical qubits in a planar network of physical qubits. The unit of this architecture has recently been implemented in superconducting circuits [23].

Numerical simulations play a crucial role in advancing experimental development [23–26] of KPO-based quantum annealing. They can be utilized to provide theoretical evidence by reproducing experimental results and to optimize experiments by evaluating the impact of each parameter. Simulating the dynamics of KPOs, however,

is computationally demanding due to large photon number n in their coherent states. For example, a recent experiment for two KPOs was operated at an average photon number of $n = 10$, requiring up to 30 basis states per KPO when simulated in a Fock basis [26]. The high computational complexity stands in contrast to the fact that this system only has two qubits. There should be more resource-efficient numerical approaches that leverage our knowledge of the system’s dynamics, i.e., the time-dependence of large- n cat states.

Various numerical methods for handling large- n states have been proposed, but unfortunately, they are unlikely to perform well for simulating KPO-based quantum annealing. A simple approach shifts the Fock basis states with displacement operators [27], but, a priori, it does not work with a time-dependent displacement. ‘The dynamic shifted Fock’ method [28] can avoid this limitation, but cannot efficiently handle large- n cat states. There are also more general approaches that express quantum states in non-orthogonal coherent-state bases [29–31], and that compress the local Hilbert-space dimensions in tensor-network states [32]. However, it remains difficult to assess whether these methods can be applied successfully to KPO-based quantum annealing. Lastly, large Hilbert spaces can be avoided by estimating the evolution of expectation values via a cumulant expansion [33], but this method has been shown to fail for some problems [34].

To overcome these difficulties, this paper derives a simple effective model, describing each KPO using a spin-1/2 degree of freedom. The model assumes that the states of KPOs are sufficiently close to a basis of coherent states $\{|\pm\alpha\rangle\}$, and that α , including its time dependence, can be estimated from the ideal quantum annealing. Reducing the system’s degrees of freedom to spin-1/2 significantly simplifies numerical simulations. This simplification is also useful for understanding the annealing dynamics. The present model is simpler than the previously proposed model for KPOs [35], yet it provides a more accurate approximation and is better suited for numerical calculations.

* l.stenzel@parityqc.com

This article is organized as follows. In Sec. II, we derive the terms of the effective Hamiltonian, and estimate their time-dependent parameters. In Sec. III, we demonstrate that the effective model can predict outcomes for different annealing schedules and realistic experimental parameters. Finally, we conclude the article in Sec. IV.

Our simulations are implemented in Python using the QuTiP library [36], and the code, and all data shown in this paper are available online [37].

II. METHOD

This section introduces a spin-1/2 Hamiltonian with rescaled coefficients, which reproduces the dynamics of adiabatic KPO-based quantum annealing. The spin model has two advantages compared to the exact Fock-space Hamiltonian. First, the spin model uses a time-independent computational basis, which can be interpreted more easily. Second, the spin Hamiltonian can be simulated more efficiently on classical hardware: For the Fock-space Hamiltonian, the number of required basis states per KPO is determined by the final photon number $\langle \hat{n} \rangle \approx \alpha^2$. For realistic experimental settings, $\mathcal{O}(10)$ states may be required per KPO; Simulating a spin-1/2 model thus allows us to simulate at least three- or four-times larger systems.

A. Projection onto Spin States

The spin model assumes that the state $|\psi(t)\rangle$ of a KPO at time t lies within the space spanned by coherent states $|\pm\alpha(t)\rangle$. We explain the estimation of α based on ideal quantum annealing for a specific Hamiltonian in Sec. II C.

Since $\langle \alpha | -\alpha \rangle \neq 0$, we will instead use the cat-state basis for deriving the effective operators,

$$\begin{aligned} |C_+(\alpha)\rangle &:= \mathcal{N}_+ (|\alpha\rangle + |-\alpha\rangle) \\ &= (\cosh \alpha^2)^{-1/2} \sum_{n=0}^{\infty} \frac{\alpha^{2n}}{\sqrt{(2n)!}} |2n\rangle_F, \\ |C_-(\alpha)\rangle &:= \mathcal{N}_- (|\alpha\rangle - |-\alpha\rangle) \\ &= (\sinh \alpha^2)^{-1/2} \sum_{n=0}^{\infty} \frac{\alpha^{2n+1}}{\sqrt{(2n+1)!}} |2n+1\rangle_F, \end{aligned} \quad (1)$$

where $|n\rangle_F$ denotes the Fock-basis state with n particles, and \mathcal{N}_{\pm} are the respective normalization constants. To make the distinction between Fock- and spin-space more clear, we define the projective transformation as

$$\hat{P}(\alpha) = |-\rangle \langle C_-(\alpha)| + |+\rangle \langle C_+(\alpha)|, \quad (3)$$

where $\{|\pm\rangle\}$ denote the Pauli- $\hat{\sigma}^x$ eigenstates of a spin-1/2 degree of freedom. For a Fock state $|\psi\rangle$, the approximation of the spin model is thus valid if

$$\langle \psi | \hat{P}^\dagger(\alpha) \hat{P}(\alpha) | \psi \rangle \approx 1. \quad (4)$$

In the spin basis, we want to compute the time evolution of $|\phi(t)\rangle := \hat{P} |\psi(t)\rangle$, i.e.,

$$\begin{aligned} \frac{d}{dt} |\phi\rangle &= \hat{P} \frac{d}{dt} |\psi\rangle + \left(\frac{d}{dt} \hat{P} \right) |\psi\rangle \approx \\ &\left[\hat{P} \left(\frac{1}{i\hbar} \hat{H}_F \right) \hat{P}^\dagger + \left(\frac{d}{dt} \hat{P} \right) \hat{P}^\dagger \right] |\phi\rangle \equiv \frac{1}{i\hbar} \hat{H}_S |\phi\rangle, \end{aligned} \quad (5)$$

where \hat{H}_F is the original Hamiltonian, typically represented in the Fock basis, and we use the approximation corresponding to Eq. (4). The effective Hamiltonian \hat{H}_S can be further simplified by the fact that the second term is diagonal,

$$\begin{aligned} \left(\frac{d}{dt} \hat{P}(\alpha) \right) \hat{P}^\dagger(\alpha) &= \frac{d\alpha}{dt} \left(\partial_{\tilde{\alpha}} \hat{P}(\tilde{\alpha}) \right)_\alpha \hat{P}^\dagger(\alpha) = \\ &\frac{d\alpha}{dt} \left(|+\rangle \partial_{\tilde{\alpha}} \langle C_+(\tilde{\alpha}) | C_+(\alpha) \rangle \Big|_{\tilde{\alpha}=\alpha} \langle +| \right. \\ &\quad \left. + |-\rangle \partial_{\tilde{\alpha}} \langle C_-(\tilde{\alpha}) | C_-(\alpha) \rangle \Big|_{\tilde{\alpha}=\alpha} \langle -| \right), \end{aligned} \quad (6)$$

which can be seen from the definition of the cat states, Eqs. (1) and (2), only containing either even or odd Fock states. Furthermore, the diagonal terms in Eq. (6) also vanish: This can be seen by computing the derivatives and overlaps explicitly, or simply by observing that the function

$$f_s(\tilde{\alpha}) := \langle C_s(\tilde{\alpha}) | C_s(\alpha) \rangle, \quad s \in \{+, -\}, \quad \alpha, \tilde{\alpha} \in \mathbb{R}_{\geq 0} \quad (7)$$

has a maximum at $\tilde{\alpha} = \alpha$, and thus the derivative $\partial_{\tilde{\alpha}} f_s|_{\alpha} = 0$ vanishes. Thus, the spin-1/2 Hamiltonian can be obtained simply by projection, and the time-dependence of $\alpha(t)$ does not even matter,

$$\hat{H}_S(\alpha) = \hat{P}(\alpha) \hat{H}_F \hat{P}^\dagger(\alpha). \quad (8)$$

B. Fock Operators in Spin Basis

Let us now compute the terms of the KPO Hamiltonian explicitly. The particle annihilator becomes a combination of two Pauli operators:

$$\begin{aligned} \hat{P}(\alpha) \hat{a} \hat{P}^\dagger(\alpha) &= |-\rangle \langle + | \alpha \sqrt{\tanh \alpha^2} + \alpha \sqrt{\coth \alpha^2} |+\rangle \langle -| \\ &= \frac{\alpha}{2} \left[\left(\sqrt{\tanh \alpha^2} - \sqrt{\coth \alpha^2} \right) i \hat{\sigma}^y \right. \\ &\quad \left. + \left(\sqrt{\tanh \alpha^2} + \sqrt{\coth \alpha^2} \right) \hat{\sigma}^z \right]. \end{aligned} \quad (9)$$

The single-photon drive is thus diagonal in the computational basis,

$$\begin{aligned} \hat{P}(\alpha) (\hat{a} + \hat{a}^\dagger) \hat{P}^\dagger(\alpha) &= \alpha \left(\sqrt{\tanh \alpha^2} + \sqrt{\coth \alpha^2} \right) \hat{\sigma}^z. \end{aligned} \quad (10)$$

The particle-number operator corresponds to a Pauli- σ^x operator, plus a constant offset,

$$\hat{P}\hat{n}\hat{P}^\dagger = \frac{\alpha^2}{2} [(\tanh \alpha^2 - \coth \alpha^2) \hat{\sigma}^x + (\tanh \alpha^2 + \coth \alpha^2) \mathbb{1}] . \quad (11)$$

We note that

$$\hat{P}(\alpha)\hat{a}^2\hat{P}^\dagger(\alpha) = \alpha^2, \quad (12)$$

and thus both the two-photon drive,

$$\hat{P}(\alpha) \left(\hat{a}^{\dagger 2} + \hat{a}^2 \right) \hat{P}^\dagger(\alpha) = 2\alpha^2, \quad (13)$$

and the Kerr nonlinearity,

$$\hat{P}(\alpha)\hat{a}^{\dagger 2}\hat{a}^2\hat{P}^\dagger(\alpha) = \alpha^4, \quad (14)$$

do not contribute directly to the spin dynamics.

C. Estimating $\alpha(t)$

To use the results from Sec. II B, we need to estimate $\alpha(t)$ from the parameters of the Fock-space Hamiltonian. For concreteness, we consider the 2-KPO Hamiltonian realized in a recent experiment [26]:

$$\hat{H}_{K_j}(t) = \frac{K_j}{2} \hat{a}_j^{\dagger 2} \hat{a}_j^2 + \Delta(t) \hat{n}_j + \frac{p_j(t)}{2} \left(\hat{a}_j^{\dagger 2} + \hat{a}_j^2 \right), \quad (15)$$

$$\hat{H}_{\Omega_j}(t) = \Omega_j(t) \left(\hat{a}_j^\dagger + \hat{a}_j \right), \quad (16)$$

$$\hat{H}_g = g \left(\hat{a}_0^\dagger \hat{a}_1 + \hat{a}_0 \hat{a}_1^\dagger \right), \quad (17)$$

$$\hat{H}(t) = H_g + \sum_j \hat{H}_{\Omega_j}(t) + \hat{H}_{K_j}(t), \quad (18)$$

where the index $j = 0/1$ represents the labels of the KPOs, K_j is the Kerr nonlinearity, p_j is the two-photon pump strength, Ω_j is the one-photon drive strength, g is the interaction strength between the KPOs. With the definitions used in [26], i.e., $K_j < 0$, $\Delta(0) < -|g|$, and $p_j(0) = 0$, the vacuum is the unique maximal-energy state of $\hat{H}(0)$ [15]. For adiabatic annealing, the system should remain in the highest-energy state as the system parameters are varied. Thus, we expect $\alpha(t)$ to be given by

$$\alpha(t) \approx \arg \max_{\alpha} \max_{\psi} \langle \psi | \hat{P}(\alpha) \hat{H}(t) \hat{P}^\dagger(\alpha) | \psi \rangle, \quad (19)$$

where we have to perform a joint optimization for all KPOs simultaneously. A similar approach, using products of coherent states as trial wave functions, was used by Kanao and Goto [38] to estimate the effect of spatially inhomogeneous α on the annealing outcomes.

The maximization in Eq. (19) only requires partial diagonalization of the spin Hamiltonian $\hat{P}\hat{H}\hat{P}^\dagger$, such that

determining α is typically numerically cheaper than actually solving the master equation.

Alternatively, one can assume that the problem Hamiltonian, i.e., the terms \hat{H}_{Ω_j} and \hat{H}_g , are small compared to \hat{H}_{K_j} , such that it suffices to use the bare KPO Hamiltonian Eq. (15) in the optimization Eq. (19). We find this approach yields quite similar results to the following analytical approximation [15], especially for larger p , i.e., at the end of the annealing process,

$$\alpha \approx \sqrt{\frac{\Delta \tanh(p/\Delta) - p}{K}}. \quad (20)$$

III. NUMERICAL RESULTS

This section demonstrates the usefulness of the spin-1/2 model by simulating multi-KPO systems in experimentally realistic regimes, and compare the results with the ones using the Fock basis. Sec. III A studies a family of two-KPO systems, closely resembling a recent experiment of some of the authors [26]. The following Sec. III B then shows results for a four-KPO interaction, which could be a building block for quantum optimization using the Parity architecture [18].

We test the spin model's ability to predict the final state of quantum annealing for different annealing schedules. While the spin model cannot exactly reproduce the Fock results, as it cannot represent leakage out of the cat-state basis, it shows the correct behavior, indicating its usefulness for parameter and schedule optimization.

A. 2-KPO Simulations

In this section, we simulate a family of two-KPO systems and try to use the spin-1/2 model to optimize the schedule of the single-photon drive. The setup is chosen to mirror recent experiments by Yamaji *et al.* [26]: $K_0/2\pi = K_1/2\pi = -12.6$ MHz, $p_0/2\pi = 148$ MHz, $p_1/2\pi = 169$ MHz, $g/2\pi = 6.9$ MHz, and $\Delta(0)/2\pi = -20$ MHz. The annealing schedule is chosen as in Ref. [26], and stated explicitly in Sec. A. We use α given by Eq. (19).

We also include photon loss and dephasing terms similar to Yamaji *et al.* [26], i.e., simulating the Lindblad equation

$$\frac{d\rho}{dt} = -\frac{i}{\hbar} [\hat{H}, \rho] + \sum_j \left(\frac{\kappa_j}{2} \mathcal{D}[\hat{a}_j, \rho] + \gamma \mathcal{D}[\hat{a}_j^\dagger \hat{a}_j, \rho] \right), \quad (21)$$

where the dephasing rate is chosen as $\gamma/2\pi = 7.7$ kHz, the photon-loss rates as $\kappa_0/2\pi = 1.1$ MHz, and $\kappa_1/2\pi = 1.3$ MHz, and

$$\mathcal{D}[\hat{O}, \rho] := \hat{O}\rho\hat{O}^\dagger - \frac{1}{2} \left(\hat{O}^\dagger\hat{O}\rho + \rho\hat{O}^\dagger\hat{O} \right). \quad (22)$$

The Lindblad equation for the effective spin model can be obtained using the operators derived in Sec. II B, under the assumption of Eq. (4).

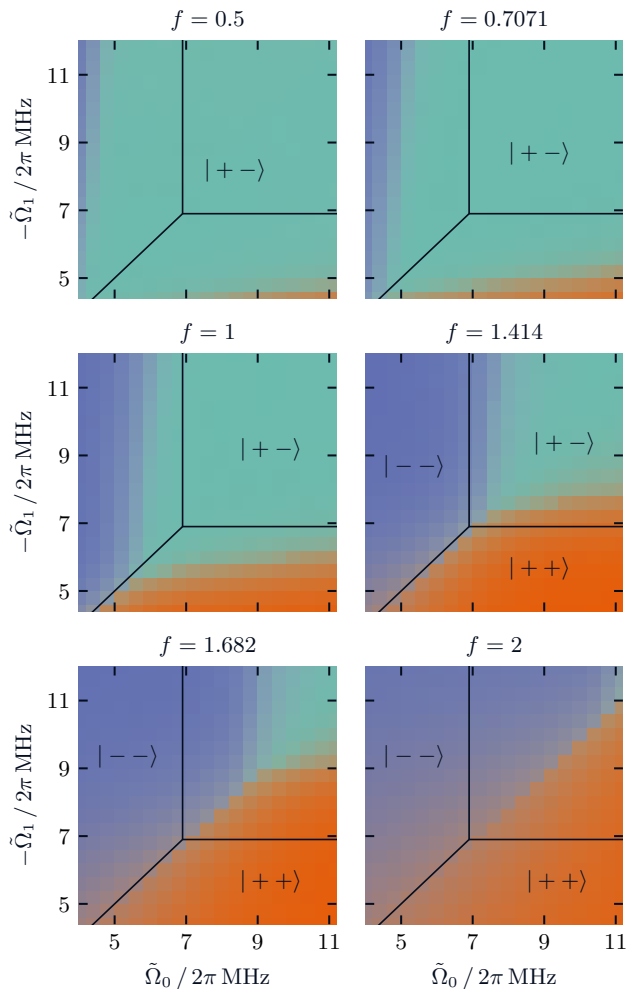


FIG. 1. Most likely annealing outcomes as function of single-photon drive strengths $\tilde{\Omega}_{0,1}$, and single-photon drive schedules, parameterized by f . Data are computed using the spin model. The colors on the heat map represent the most likely final states. The black lines indicate the ground-state boundaries of the final Hamiltonian, for all values of f . The simulations suggest that the outcomes deviate from ideal state boundaries, indicating that our assumption of adiabaticity, used in Eq. (19), can be violated.

We rescale the strength of the single-photon drive by the maximal α , as approximated by Eq. (20),

$$\tilde{\Omega}_j := \Omega_j \prod_{l \neq j} \sqrt{-K_l/p_l} \approx \Omega_j \prod_{l \neq j} \alpha_l(T_s)^{-1}, \quad (23)$$

such that $\tilde{\Omega}$ is comparable with the interaction strength g : For coherent states, the expectation value of the interaction term is $\langle \hat{H}_g \rangle = 2g \prod_j \alpha_j$, and for the single-photon drive $\langle \hat{H}_{\Omega_j} \rangle = 2\Omega_j \alpha_l \approx 2\tilde{\Omega}_j \prod_j \alpha_j$. This approach does not directly translate to KPO systems with multiple interaction terms [38].

In Fig. 1 we study the case of competition between local

fields $\tilde{\Omega}_j$ and interaction g . We consider $g/2\pi = 6.9$ MHz which favors parallel ‘alignment’ of the coherent states, but choose opposite signs for the single-photon drives $\tilde{\Omega}_0$ and $\tilde{\Omega}_1$. In the subplots we observe that the most-likely final state strongly depends on the schedule of the local fields $\tilde{\Omega}$. We can understand this by revisiting the motivation behind rescaling the local fields in Eq. (23): As $\alpha(t)$ changes during the annealing process, the interaction term scales as $\alpha_0(t)\alpha_1(t)$, while the local-field term is proportional to $\langle \hat{H}_{\Omega_j(t)} \rangle \propto t^f \alpha_j(t)$. For a strictly adiabatic annealing process, the details of the schedule should not matter. However, we saw in Sec. II B that all terms in the Hamiltonian become diagonal for large α , and thus the system can no longer respond to changes of the local fields.

The spin model is based on two assumptions: The instantaneous ground state lies within the coherent-state basis $|\pm\alpha(t)\rangle$, and $\alpha(t)$ corresponds to the instantaneous maximal energy state. Neither assumption is strictly true, here: Due to dephasing, there is leakage out of the coherent-state basis. And the final states depend on the annealing schedule, meaning that the system does not always realize the maximal energy state.

The fact that the assumptions are not true means that the model’s validity cannot be guaranteed in the above setting mirroring the experiment. However, if the approximations in introducing the spin model have not distorted the schedule dependency, practical validity of the model can be found. Comparing the simulation results of the spin model and the Fock model should clarify this point.

Here, we show that the predictions of the spin model are fairly accurate. In Fig. 2 we compare the spin-model results with simulations in a Fock basis with 27 and 30 basis states for KPO 0 and 1, respectively. We observe that the spin model tends to overestimate the probability for the most-likely state. This is likely a consequence of leakage out of the coherent-state basis due to dephasing γ , which cannot be described accurately in the spin model. However, the spin-1/2 model accurately predicts the most likely final state, and, in particular, the transition between different states as function of $\tilde{\Omega}_1$. This finding suggests that our spin model is useful for partially optimizing experiments, although the valid parameter range is limited, as discussed below.

For larger exponents $f \geq 1.5$ we observe cusps in the spin-model results in Fig. 2, which do not appear to exist in the Fock simulations. We suspect this may be related to our method of estimating α , see Eq. (19): For larger exponents f , the local fields $\tilde{\Omega}$ change more rapidly at the end of the annealing process; Since $p(t)$, and thus $\alpha(t)$, are larger, the coupling between the $|\pm\alpha\rangle$ states is weak, and the system can no longer follow the maximal energy state.

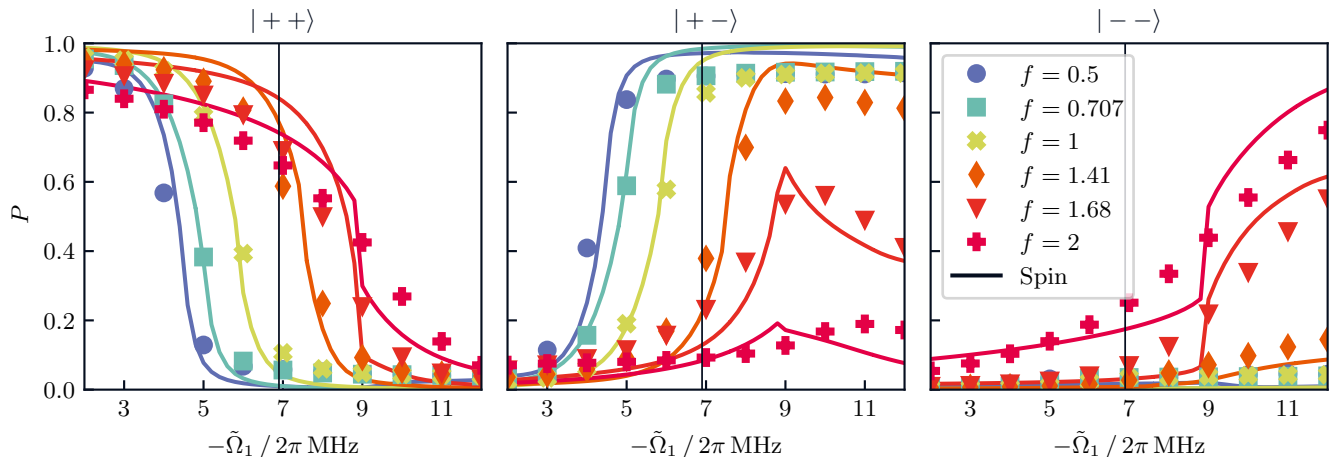


FIG. 2. Comparison of Fock and spin simulation for two KPOs. Spin simulations correspond to data shown in Fig. 1 for fixed $\tilde{\Omega}_0/2\pi = 9$ MHz. Markers indicate Fock simulations, while the solid lines are results of the spin model. Probabilities for state $| - + \rangle$ are very close to zero for all methods and parameters, and are thus not shown. The black, vertical line indicates the single-photon drive strength $\tilde{\Omega}_1$ where $| ++ \rangle$ and $| + - \rangle$ are degenerate in energy. The spin model tends to overestimate the probability of the most likely spin configuration. However, the spin model can quite accurately predict the transition point, i.e., the value of $\tilde{\Omega}_1$ where the most-likely state changes. For $f \geq 1.68$ we observe cusps in the spin results, which appear not to be present in the Fock-space simulations.

B. 4-KPO Simulations

We want to show the versatility of the spin-1/2 model by simulating a larger system of four KPOs, which are interacting as

$$\hat{H}_g = g(\hat{a}_0^\dagger \hat{a}_1^\dagger \hat{a}_2 \hat{a}_3 + \hat{a}_0 \hat{a}_1 \hat{a}_2^\dagger \hat{a}_3^\dagger). \quad (24)$$

The four-body interaction for KPOs has been studied theoretically [10, 39, 40], and has recently been implemented [23]. Such system could, e.g., realize the Parity architecture [10, 18].

We use very similar parameters as in Sec. III A, and used experimentally by Yamaji *et al.* [26]; I.e., a Kerr coefficient of $K/2\pi = -12.6$ MHz, initial detuning $\Delta(0)/2\pi = -20$ MHz ramped linearly to $\Delta(t \geq t_s) = 0$, and a dephasing rate of $\gamma/2\pi = 7.7$ kHz. We also use comparable photon loss-rates $\kappa/2\pi = (0.9, 1.1, 1.3, 1.5)$ MHz, but a slightly faster annealing schedule using times $T_s = 0.5$ μ s, $T_{sp} = 0.1$ μ s, $T_{rd} = 0.1$ μ s, $T_r = 0.1$ μ s, see Fig. 4 for the definition of the parameters. The shorter total duration is primarily chosen to ease numerical simulation demands.

Furthermore, to make Fock-space simulations numerically more tractable, we reduce the two-photon pump strength to $\mathbf{p}/2\pi = (10, 20, 15, 14)$ MHz, and thus reducing the size of the coherent states to $\alpha \in [0.89, 1.26]$. This reduces the number of required Fock basis states per KPO to about 8, while achieving the same accuracy as in the previous Sec. III A. As a side effect, the reduced α should decrease the influence of dephasing γ , decreasing the leakage out of the $|\pm\alpha\rangle$ basis. In any case, these parameters would likely not be optimal for future experiments, because measuring small- α coherent states would be more

difficult, and a larger overlap $|\langle \alpha | -\alpha \rangle|$ may decrease the fidelity. We also choose the rescaled single-photon drive strength (cf. Eq. (23)) to be as strong as the four-body interaction, $\tilde{\Omega}_0 = \tilde{\Omega}_2 = -\tilde{\Omega}_1 = g = 4\pi$ MHz, and vary the strength of the last KPO's single-photon drive $\tilde{\Omega}_3$.

In Fig. 3 we find that the exponent f of the single-photon drive schedule (cf. Fig. 4) has a much smaller impact on the outcome than what we saw in Sec. III A. We attribute this to the smaller value of α : As the overlap $|\langle \alpha | -\alpha \rangle|^2$ is larger, the spin evolution is not ‘frozen’ at the end of the schedule. And thus, the states at intermediate times during the annealing process do not impact the final outcome as much. We find the spin model reproduces the correct behavior of the outcome probabilities both as a function of single-photon drive strength $\tilde{\Omega}_3$ and schedule parameter f . Note that the Fock results are obtained by averaging 400 Monte-Carlo trajectories [41, 42], and thus have a statistical error.

IV. CONCLUSION AND OUTLOOK

In this paper, we propose a simple method for approximating the dynamics of quantum annealers using KPOs. By projecting onto a time-dependent, two-dimensional basis spanned by coherent states, we derive an effective Hamiltonian with time-dependent coefficients. This allows us to interpret KPO-based quantum annealing in terms of a system of qubits.

The spin model can also be used for more efficient numerical simulations: For the parameters used in a recent experiment, 20-30 Fock basis states are required for

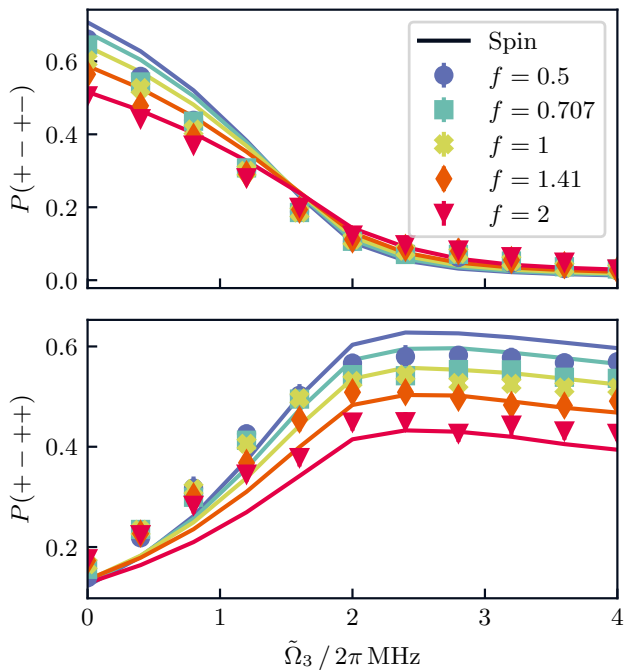


FIG. 3. Outcome probabilities for the ideal ground states as functions of the local single-photon drive on KPO 3. The most likely state changes from $|+ - - \rangle$ to $|+ - + \rangle$ for larger $\tilde{\Omega}_3$. Markers correspond to simulations in the Fock space, while the solid lines are the result of simulations in the spin model. Compared to Fig. 2, the schedule of the local fields, parameterized by f , has a much smaller influence on the observed results.

accurate results. Thus, the spin model allows us to study systems of more than four times the number of KPOs with comparable memory and compute requirements. Note that there is some computational overhead for estimating α for each KPO, see Sec. II C, but this cost was subleading for all of our simulations.

We show in Sec. III that the spin model can predict the outcome of different annealing schedules, and could thus be useful for optimizing future experiments. There are no free parameters in the effective model, however the method for estimating α , see Sec. II C, affects the results.

Further research is required for controlling the spin model's error. One way could be adding further states to the $|\pm\alpha\rangle$ basis, similar to other methods using coherent-state bases for numerical simulations [28, 30, 31]. However, such an approach would yield more complicated expressions, and require a different implementation. The error of the spin model can be estimated more simply, by simulating a subset of KPOs in a Fock basis. This is particularly useful for single-KPO observables, but it can also serve to compute the leakage out of the cat basis, giving an insight into the validity of the spin model.

ACKNOWLEDGMENTS

R.M., T.Y., and M.S. are grateful to Y. Igarashi, Y. Kawakami, and T. Yamamoto for useful discussions. L.S. thanks P. Aumann for useful discussions.

-
- [1] P. Krantz, M. Kjaergaard, F. Yan, T. P. Orlando, S. Gustavsson, and W. D. Oliver, *Appl. Phys. Rev.* **6**, 021318 (2019).
- [2] J. Koch, T. M. Yu, J. Gambetta, A. A. Houck, D. I. Schuster, J. Majer, A. Blais, M. H. Devoret, S. M. Girvin, and R. J. Schoelkopf, *Phys. Rev. A* **76**, 042319 (2007).
- [3] P. T. Cochrane, G. J. Milburn, and W. J. Munro, *Phys. Rev. A* **59**, 2631 (1999).
- [4] S. Puri, S. Boutin, and A. Blais, *npj Quantum Inf.* **3**, 18 (2017).
- [5] J. Guillaud and M. Mirrahimi, *Phys. Rev. X* **9**, 041053 (2019).
- [6] T. Kadowaki and H. Nishimori, *Phys. Rev. E* **58**, 5355 (1998).
- [7] T. Albash and D. A. Lidar, *Rev. Mod. Phys.* **90**, 15002 (2018).
- [8] P. Hauke, H. G. Katzgraber, W. Lechner, H. Nishimori, and W. D. Oliver, *Rep. Prog. Phys.* **83**, 054401 (2020).
- [9] H. Goto, *Sci. Rep.* **6**, 21686 (2016).
- [10] S. Puri, C. K. Andersen, A. L. Grimsmo, and A. Blais, *Nat. Commun.* **8**, 15785 (2017).
- [11] S. E. Nigg, N. Lörch, and R. P. Tiwari, *Sci. Adv.* **3**, e1602273 (2017).
- [12] P. Zhao, Z. Jin, P. Xu, X. Tan, H. Yu, and Y. Yu, *Phys. Rev. Applied* **10**, 024019 (2018).
- [13] T. Onodera, E. Ng, and P. L. McMahon, *npj Quantum Inf.* **6**, 48 (2020).
- [14] H. Goto, *J. Phys. Soc. Jpn.* **88**, 061015 (2019).
- [15] H. Goto, Z. Lin, and Y. Nakamura, *Sci. Rep.* **8**, 1 (2018).
- [16] Y. Zhang and M. I. Dykman, *Phys. Rev. A* **95**, 053841 (2017).
- [17] H. Goto and T. Kanao, *Commun. Phys.* **3**, 235 (2020).
- [18] W. Lechner, P. Hauke, and P. Zoller, *Sci. Adv.* **1**, e1500838 (2015), <https://www.science.org/doi/pdf/10.1126/sciadv.1500838>.
- [19] K. Ender, R. ter Hoeven, B. E. Niehoff, M. Drieb-Schön, and W. Lechner, *Quantum* **7**, 950 (2023).
- [20] M. Drieb-Schön, K. Ender, Y. Javanmard, and W. Lechner, *Quantum* **7**, 951 (2023).
- [21] M. Fellner, K. Ender, R. ter Hoeven, and W. Lechner, *Quantum* **7**, 952 (2023).
- [22] R. ter Hoeven, B. E. Niehoff, S. S. Kale, and W. Lechner, *Quantum Sci. Technol.* **9**, 035056 (2024).
- [23] Y. Kawakami, T. Yamaji, A. Yamaguchi, Y. Kano, T. Aoki, A. Taguchi, K. Endo, T. Satoh, A. Morioka, Y. Igarashi, M. Shirane, and T. Yamamoto, *arXiv* (2025), 2512.00446.
- [24] T. Yamaji, S. Kagami, A. Yamaguchi, T. Satoh,

- K. Koshino, H. Goto, Z. R. Lin, Y. Nakamura, and T. Yamamoto, Phys. Rev. A **105**, 023519 (2022).
- [25] T. Yamaji, M. Shirane, and T. Yamamoto, IEICE TRANS. ELECTRON. **E105-C**, 283 (2022).
- [26] T. Yamaji, S. Masuda, Y. Kano, Y. Kawakami, A. Yamaguchi, T. Satoh, A. Morioka, Y. Igarashi, M. Shirane, and T. Yamamoto, Quantum annealing in capacitively coupled Kerr parametric oscillators using frequency-chirped drives (2025), arXiv:2506.23539 [quant-ph].
- [27] C. Chamberland, K. Noh, P. Arrangoiz-Arriola, E. T. Campbell, C. T. Hann, J. Iverson, H. Putterman, T. C. Bohdanowicz, S. T. Flammia, A. Keller, G. Refael, J. Preskill, L. Jiang, A. H. Safavi-Naeini, O. Painter, and F. G. Brandão, PRX Quantum **3**, 010329 (2022).
- [28] A. Mercurio, Y.-T. Huang, L.-X. Cai, Y.-N. Chen, V. Savona, and F. Nori, Quantum **9**, 1866 (2025).
- [29] A. Vukics, Comput. Phys. Commun. **183**, 1381 (2012).
- [30] S. Krämer, *Simulating open quantum systems with high photon numbers in coherent bases*, Master's thesis, University Innsbruck (2011).
- [31] D. S. Schlegel, F. Minganti, and V. Savona, Coherent-State Ladder Time-Dependent Variational Principle for Open Quantum Systems (2023), arXiv:2306.13708 [quant-ph].
- [32] T. Köhler, J. Stolpp, and S. Paeckel, SciPost Phys. **10**, 10.21468/scipostphys.10.3.058 (2021).
- [33] D. Plankensteiner, C. Hotter, and H. Ritsch, Quantum **6**, 617 (2022).
- [34] J. Kerber, H. Ritsch, and L. Ostermann, The Cumulants Expansion Approach: The Good, The Bad and The Ugly (2025), arXiv:2511.20115 [quant-ph].
- [35] R. Miyazaki, Phys. Rev. A **105**, 062457 (2022).
- [36] N. Lambert, E. Giguère, P. Menczel, B. Li, P. Hopf, G. Suárez, M. Gali, J. Lishman, R. Gadhvi, R. Agarwal, A. Galicia, N. Shammah, P. Nation, J. Johansson, S. Ahmed, S. Cross, A. Pitchford, and F. Nori, Phys. Rep. **1153**, 1 (2026).
- [37] L. Stenzel, Spin-Model Simulations for KPO Annealing (2026).
- [38] T. Kanao and H. Goto, npj Quantum Inf. **7**, 18 (2021).
- [39] R. Miyazaki and T. Yamamoto, Phys. Rev. A **111**, 062612 (2025).
- [40] Y. Matsuzaki, Y. Mori, A. Yamaguchi, Y. Kawakami, and T. Yamamoto, Jpn. J. Appl. Phys. **64**, 052002 (2025).
- [41] J. Dalibard, Y. Castin, and K. Mølmer, Phys. Rev. Lett. **68**, 580 (1992).
- [42] R. Dum, P. Zoller, and H. Ritsch, Phys. Rev. A **45**, 4879

(1992).

Appendix A: Annealing Schedule

The annealing schedule also mimics the experiment [26], and is sketched in Fig. 4: One- and two-photon pump strengths are increased in $T_s = 0.4 \mu\text{s}$ to their respective final values. We scale the two-photon pump as in the experiment as $t^{2.5}$, but consider different monomial schedules for the single-photon drive $\Omega \propto t^f$. During the same time, the detuning $\Delta(t)$ is linearly increased to zero.

After a hold time of $T_{\text{sp}} = 0.1 \mu\text{s}$, the single-photon pump $\Omega(t)$ is again decreased to zero. In the experiment, this is required to avoid interference with the readout.

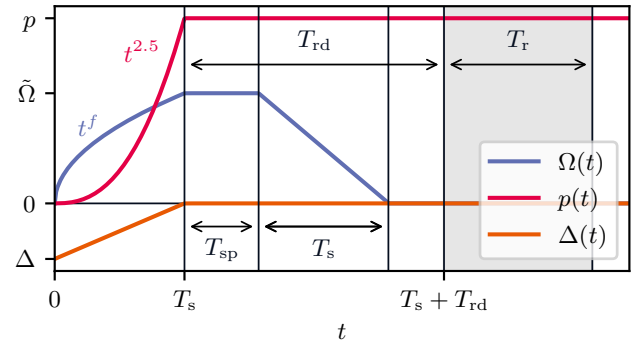


FIG. 4. Illustration of the schedules used in our simulations. The parameters are taken directly from the recent experiment [26]. The state is prepared during T_s , then the single-photon drive $\Omega(t)$ needs to be turned off again, before the KPOs are measured during time T_r , indicated by the shaded region. We use a monomial schedule with exponent 2.5 for the two-photon drive $P(t)$, as in the experiment [26], but vary the exponent f of the local field-schedule $\Omega(t)$.

The readout begins at $T_s + T_{\text{rd}}$, where $T_{\text{rd}} = 0.6 \mu\text{s}$, and lasts for $T_r = 0.4 \mu\text{s}$. Numerically, we simulate the readout by time-averaging the expectation values over T_r .